Vorticity Dissipation by Western Boundary Currents in the Presence of Outcropping Layers

ERIC P. CHASSIGNET

RSMAS/MPO, University of Miami, Miami, Florida

(Manuscript received 22 December 1993, in final form 16 June 1994)

ABSTRACT

In an exploration of the dynamics of current separation and vorticity dissipation in a two-layer model, the following is found. 1) Results obtained in a barotropic context remain valid; namely, two major dissipation regimes can be found: either a "loop current" or a recirculating gyre. 2) A transition from one regime to the other can be achieved if one increases the strength of the front associated with the outcrop, regardless of the specified boundary conditions. 3) Separation will depend upon the choice of lateral boundary conditions if the upper-layer flow is not highly inertial.

1. Introduction

In this paper, it will be shown in the context of a two-layer numerical model that the mechanism behind the separation of a western boundary current cannot be dissociated from the mechanism responsible for the dissipation process. Of particular interest is the recirculation regime that increases the eastward transport of the separated current (Hogg 1992). It is of the utmost importance to assess the factors responsible for both the separation and the recirculation, as most existing realistic numerical simulations of the North Atlantic circulation (Fig. 1) not only exhibit an overshooting Gulf Stream but also an intense stationary eddy that hugs the coast at the separation latitude. The modeled Gulf Stream separates north of this anticyclone and does not exhibit any recirculation cells resembling observations (Hogg 1992; Beckmann et al. 1994).

In the inertial limit of the steady barotropic circulation, the boundary layers are not strong enough to dissipate the total input of vorticity in the large-scale flow by the wind (Pedlosky 1987; Cessi et al. 1990). The potential vorticity of the flow entering the western boundary region differs from the interior flow that exits at approximately the separation latitude. Significant changes in potential vorticity must therefore occur in the western boundary currents before and after separation. Cessi et al. (1990, hereafter referred to as CCY) and Cessi (1991) demonstrated the existence of two limiting forms of potential vorticity dissipation, either a damped stationary Rossby wave (Moore 1963; Pedlosky 1987; Campos and Olson 1991) or an inertial recirculation (Cessi et al. 1987). The first process, namely, the closing of the circulation by a stationary Rossby wave, was proposed initially by Moore (1963). Pedlosky (1987) interpreted the role of this wave as a baffle that essentially increases the length of a streamline, thereby allowing a more efficient diffusion of potential vorticity. CCY, on the other hand, surmised that most of the potential vorticity alterations occur at the western boundary in only the first crest of the Rossby wave. They argue that the initial northward overshoot and southward plunge (called the "loop current" by CCY) is a distinct dynamical regime, and not just the first and largest oscillation of the damped Rossby wave. In the loop current, potential vorticity is modified by extending the length of the streamlines and compressing the current in order to increase dissipation. In the second process, dissipation is achieved through inertial recirculating gyres where potential vorticity is modified in the compressed streamlines of the gyres (Cessi 1991). The main difference between the two regimes is that the former, the damped stationary Rossby wave, does not produce an increased transport, that is, closed streamlines. Geometry is surmised as being the main factor in determining whether recirculating gyres, or the loop current regime, is realized. In cases where the western boundary current comes in contact with a solid wall, or a strong current of opposite direction, the formation of the loop current is prevented and an inertial recirculation is obtained (Cessi et al. 1987; Cessi 1991). A combination of these two scenarios can actually be observed in eddy-resolving general circulation models (Holland and Lin 1975; McWilliams et al. 1990; Haidvogel et al. 1991; Chassignet

Corresponding author address: Dr. Eric Chassignet, Rosenstiel School of Marine and Atmospheric Science, Division of Meteorology and Physical Oceanography, University of Miami, 4600 Rickenbacker Causeway, Miami, FL 33149-1098.

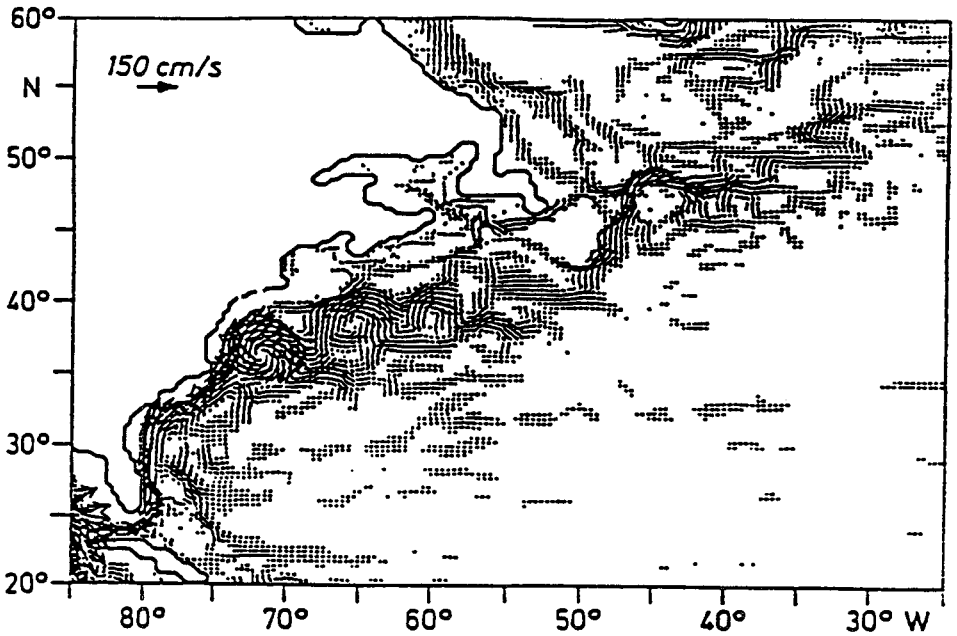

FIG. 1. Horizontal velocities at 100-m depth in the northwest Atlantic Ocean as simulated by the 1/6° resolution Community Modeling Experiment (CME) with the Gephysical Fluid Dynamics Laboratory (GFDL) numerical model [from Beckman et al. (1994)].

and Gent 1991) and in the case of a collision with a weak current of the opposite direction (Cessi 1991).

Cessi et al. (1990) and Cessi (1991) restricted their study to barotropic calculations, namely, a single layer of constant density, thereby excluding separation due to baroclinic effects and time-dependent instabilities. The question then arises as to whether the above scenarios are applicable to multilayer systems. Do the separation and associated recirculation require a baroclinic structure or is it primarily a depth-independent process? Cessi (1990) partially addressed these questions analytically with arguments based on areas of uniform potential vorticity. The recirculation was found in Cessi (1990) to extend to the bottom through baroclinic instabilities induced by the strong eastward flow associated with the upper-layer outcrop.

In this paper, the above questions are addressed in a time-dependent multilayer primitive-equation numerical model. Special emphasis is put on cases with outcropping isopycnal layers since 1) this is a natural occurence for highly inertial flows and 2) the gradient in isopycnal layer thickness associated with the outcrop will be shown to be sufficiently strong in some cases to act as a barrier or wall and to consequently provide a mechanism that permits a shift from a solution with a loop current dissipation process to one with an inertial recirculation. Investigation of regimes with outcropping is also of importance as it provides one of the simplest explanations for the separation of western boundary currents (Parsons 1969; Veronis 1973) and allows the midlatitude jet to separate south of the zero wind stress curl line (ZWCL) (Chassignet and Bleck 1993), an important property when one considers that most realistic numerical experiments to date exhibit an overshooting midlatitude jet (Thompson and Schmitz 1989; Chassignet and Gent 1991; Beckmann et al. 1994).

The layout of the paper is as follows: section 2 presents the numerical model characteristics and parameters. In section 3, the transition from a loop current regime to an inertial recirculation regime is presented in detail. Vorticity dissipation in the different regimes is discussed in section 4. Section 5 then investigates the influence of baroclinic instabilities on the dissipation process. The influence of other factors such as lateral boundary conditions and bottom drag is investigated in section 6. Finally, the results are summarized and discussed in the concluding section.

2. The numerical model

The primitive equation, pure-isopycnic model of Bleck and Boudra (1986) can be viewed as a stack of shallow water models, each consisting of a momentum and a continuity equation:

$$\frac{\partial \mathbf{v}}{\partial t} + \frac{1}{2}\nabla_\rho \mathbf{v}^2 + (\zeta + f)\mathbf{k} \times \mathbf{v}$$

$$= -\nabla_\rho M + \alpha \frac{\partial \tau}{\partial z} + A(\delta_\rho p)^{-1}\nabla_\rho \cdot \delta_\rho p \nabla_\rho \mathbf{v} - \sigma \mathbf{v}, \quad (1)$$

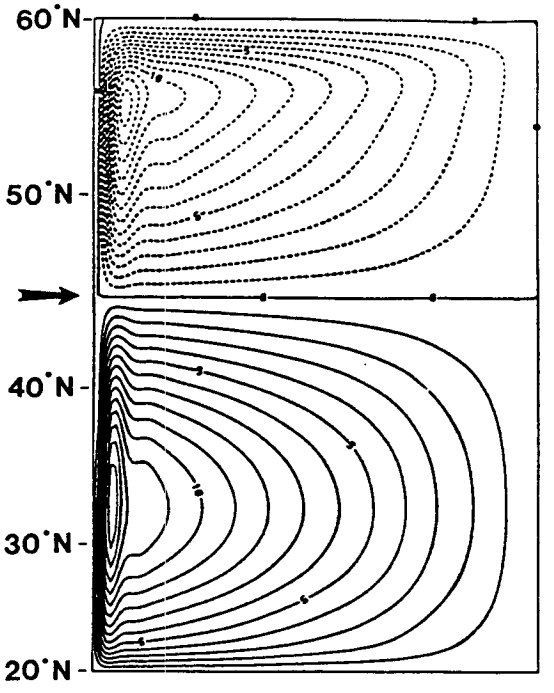

FIG. 2. Linear circulation resulting from the zonally averaged climatological wind stress derived from the COADS for the month of January. The contour interval is 1 Sv (≡ 10^6 m^3 s^{-1}). Note that the north–south dimension of the subpolar gyre appears "stretched" because of the Mercator projection. The arrow indicates the zero wind stress curl line (ZWCL).

$$\frac{\partial}{\partial t_\rho}(\delta_\rho p) + \nabla_\rho \cdot (\mathbf{v}\delta_\rho p) = 0, \qquad (2)$$

where $\zeta = v_x - u_y$ is the vorticity; $M = gz + p\alpha$ is the Montgomery potential; $\delta_\rho p$ is the thickness of a layer of constant density; $\alpha = \rho^{-1}$ the specific volume; τ is the wind stress; A is the lateral viscosity; and the bottom drag coefficient σ, when nonzero, acts only on the bottom layer. The subscript ρ indicates derivatives on surfaces of constant density. The shallow water models communicate vertically through hydrostatically transmitted pressure forces.

Horizontal velocities and vorticity are defined as mean layer properties. Pressure and geopotential are defined at the interfaces between layers. The intersection of the moving coordinate surfaces with boundaries, such as the sea surface (outcropping), is achieved by adopting the flux-corrected transport (FCT) algorithm (Boris and Book 1973; Zalesak 1979), which combines the smoothness properties of the positive-definite upstream differencing scheme with the accuracy of space-centered schemes and controls the tendency to generate negative layer thickness when solving the layer thickness prediction equation. This approach has proven very effective [see Sun et al. (1993) for a review].

The model equations are solved on a grid forming a regular mesh on a Mercator projection. North–south grid lines correspond to meridians spaced 1/3° apart. East–west grid lines run at constant latitude. The north–south spacing of grid points on the sphere changes with the spacing of meridians. The domain ranges in latitude from 21° to 59°N and the mesh size varies from 40 km in the south to 20 km in the north. The model is configured for this study with two layers in a rectangular ocean basin 30° wide and is driven by realistic zonally averaged climatological winds derived from the Comprehensive Ocean–Atmosphere Data Set (COADS) for the month of January. Because of the zonal averaging, the ZWCL on the western boundary is located farther north than in COADS. Such a forcing results in a Sverdrup circulation, which consists of a large subtropical gyre and a small subpolar gyre (Fig. 2). The wind stress is specified as a body force acting only on the layer directly beneath the surface (Chassignet and Gent 1991; Chassignet and Bleck 1993). The circulation is damped by a lateral eddy viscosity of the Laplacian form and, in some experiments, by a small linear bottom drag. The lateral boundary conditions employed on the four sidewalls are free-slip, unless explicitly stated as in section 6. The parameters for the experiments are given in Table 1.

3. The numerical experiments

According to CCY and Cessi (1991), a prerequisite for a solution that will exhibit a loop current regime is a poleward western boundary current that does not encounter either a wall or an equatorward-flowing current of comparable strength. As described in the previous section, the forcing of this numerical model is such that the resulting Sverdrup circulation satisfies

TABLE 1. For all experiments, the lateral viscosity is 600 m^2 s^{-1} and g' = .06 m s^{-2}. In the text, the subscripts s and n indicate, respectively, a total depth of 5000 m or no-slip boundary conditions.

Experiment	Initial upper-layer thickness H_1 (m)	Total depth $H = H_1 + H_2$ (m)	Wind stress multiplication factor	$\lambda = \tau_m L/g'H_1^2$	δ_I/δ_M
E1	150	10^6	1	.15	1.3
E2	100	10^6	1	.34	1.8
E3	50	10^6	1	1.35	2.6
E4	150	10^6	2	.3	2.1
E5	150	10^6	4	.6	3

this criterion, since it consists of a large subtropical gyre with a strong northward flowing western boundary current and of a small subpolar gyre with a weaker southward flowing western boundary current (Fig. 2b).

However, in the presence of outcropping layers, this scenario can actually change as the strength of the layer thickness gradient associated with the outcrop is varied. It will be shown in this section that one may observe the development of 1) a loop current regime provided that the layer thickness gradient is relatively small, or 2) in the case of a steep gradient, a regime where the vorticity transformation is achieved through an inertial recirculation. The rationale is that in the case of a strong front, the outcrop then acts as a physical barrier for the northward flowing western boundary current.

In the case of a two-layer system, the upper layer linear flow pattern is controlled by a single nondimensional number $\lambda = \tau_m L/g'H_1^2$, where τ_m is the maximum wind stress, L the basin width, g' the reduced gravity, and H_1 the mean upper-layer thickness (Veronis 1973; Huang 1984). An increase in λ leads to an increase in the size of the outcrop area and also dictates the strength of the layer thickness gradient associated with the outcrop (Huang 1984; Huang and Flierl 1987). Inclusion of the inertial terms in the momentum equations and its impact on the circulation was discussed in detail in Chassignet and Bleck (1993). All the experiments presented in this section have a very small initial upper/lower layer ratio $\delta = H_1/H_2 < 10^{-4}$, which corresponds to an "infinitely"[1] deep lower layer. Without outcropping layers, this configuration is equivalent to a reduced gravity (1½-layer) numerical model in which no baroclinic instabilities can occur (Chassignet and Cushman-Roisin 1991). When the upper-layer thickness vanishes, the wind forcing then acts directly on the lower layer and the fluid motion is barotropic. The increase in λ is first achieved through a decrease in initial upper-layer thickness in order to keep the vertically integrated Sverdrup transport constant from one experiment to the other (Table 1).

a. The loop current regime—$\lambda = 0.15$ and $\lambda = 0.34$

The parameters chosen for experiment E1 lead to $\lambda = 0.15$ (initial upper-layer thickness equal to 150 m) (Table 1). This value yields an outcrop region that spans virtually most of the cyclonically forced region and extends into the anticyclonically forced region as well (Huang 1984; Chassignet and Bleck 1993). The model is first spun up from rest for a 10-yr period (a model year consists of 360 days). It is of interest to discuss the time evolution of the upper-layer flow fields as they possess many similarities with the barotropic experiments of CCY, especially before any occurence of layer outcropping. To illustrate this phase, four instantaneous characteristic upper-layer thickness maps after, 1, 3, 8, and 10 model years, are displayed in Fig. 3.

After one year of integration (Fig. 3a), the subtropical gyre circulation is dominant and exhibits a large oscillating wave. The northward flowing western boundary current reaches the northern wall and forms a small recirculating gyre at the northwest corner of the domain. Bryan (1963) obtained a similar flow pattern in his single gyre barotropic simulations, but with a much weaker wave. This flow pattern is also in agreement with CCY, who showed that when the northward western boundary current is allowed to reach the northern wall before separation, it then drives an inertial gyre in the corner. The oscillating wave of Fig. 3a has a large amplitude, but does not penetrate far eastward.

After three years of integration (Fig. 3b), the upper-layer circulation is more intense and a southward flowing western boundary current is now present. The northward flowing western boundary current no longer reaches the northern boundary, but separates at approximately 50°N. The large oscillating wave is still present and the first southward plunge corresponds to the so-called loop current of CCY.

Outcropping of the upper layer occurs around year 7 and, after eight years of integration (Fig. 3c), the northward flowing western boundary current separation latitude is located farther south at approximately 45°N. The outcrop area now occupies most of the subpolar gyre and only the loop current part of the oscillating wave remains. After 10 years of integration, the numerical solution is in statistical equilibrium (Fig. 3d). The flow pattern consists mostly of the loop current and of a recirculation within it near the western boundary. The outcrop area is now larger and penetrates inside the oscillating wave.

After the 10-yr spinup phase, the model was further integrated for a period of 5 years. The resulting time-average streamfunctions are displayed in Fig. 4. Except for a broader jet due to time fluctuations, the overall picture is similar to the instantaneous year 10 (Fig. 3d), namely, a large wave with a large first oscillation (the loop current), which decays rapidly into the interior, and an outcrop region, which covers most of the subpolar gyre. In addition, a recirculating gyre is also present within the second crest of the oscillating wave. The separation latitude is located north of the ZWCL. In the lower layer (Fig. 4b), the circulation is of minimal strength since only a small area is directly forced by the wind.

In summary, the chosen configuration and forcing, namely, a strong subtropical gyre and a weak subpolar gyre, do lead to a flow pattern that exhibits a large standing oscillating wave, as predicted by CCY and Cessi (1991). Before any occurence of layer outcropping, the upper-layer flow patterns are in close agreement with the barotropic cases of

[1] The lower-layer initial thickness is equal to 1000 km.

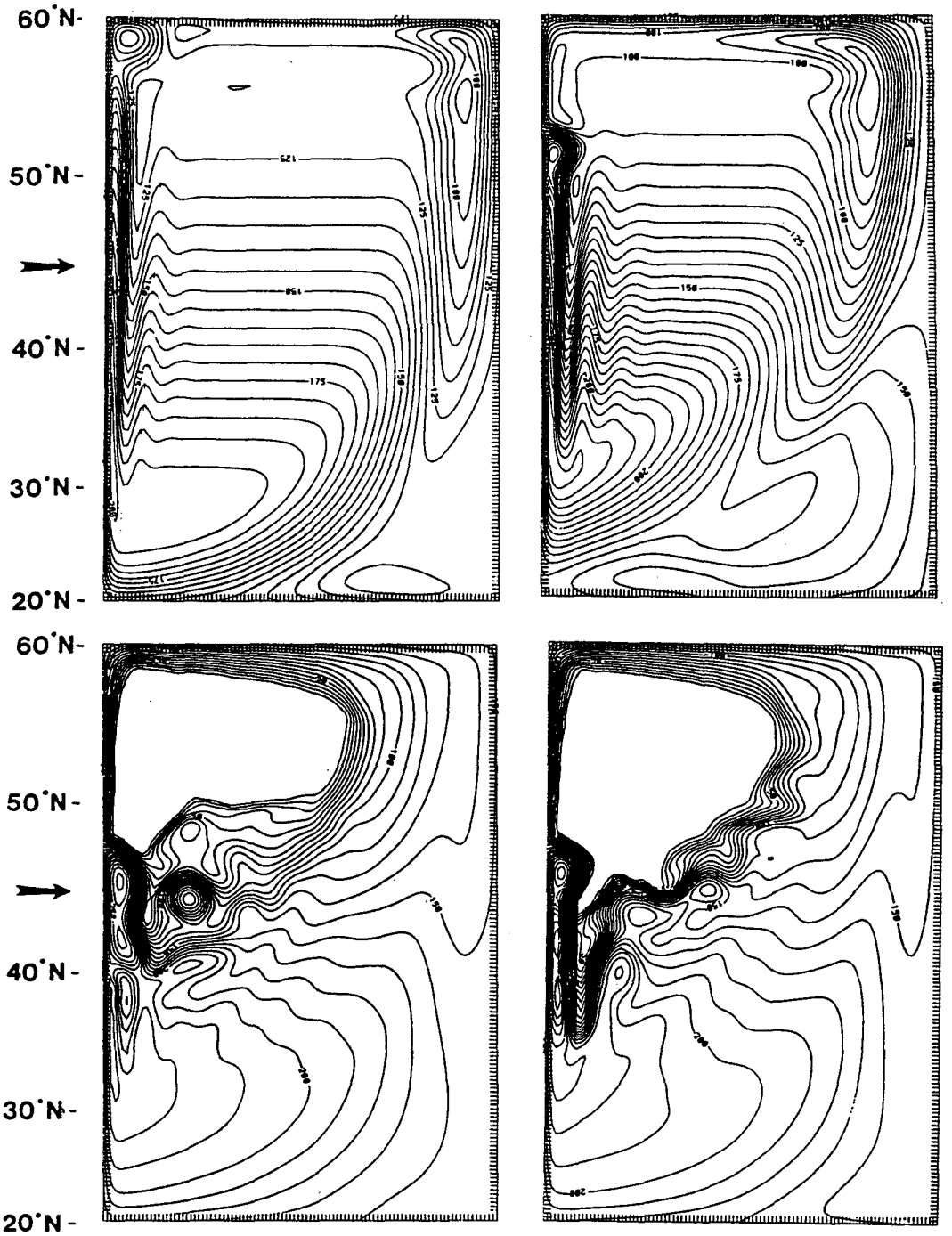

FIG. 3. Instantaneous upper-layer thickness maps for E1 after (a) 1 year, (b) 3 years, (c) 8 years, and (d) 10 years of integration. The contour interval is 5 m for (a) and (b) and 10 m for (c) and (d).

CCY and Cessi (1991) (discussed in more detail in section 4). It is only after the upper layer vanishes in the subpolar gyre that the circulations begin to differ. The large standing oscillating wave pattern or loop current remains present, however.

If one follows the rationale introduced at the beginning of this section, an increase in λ will strengthen the front associated with the outcrop area, which might then act as a barrier and induce a shift from a regime with a loop current to one with a recirculation. Experiment E2 is therefore identical to E1, except for λ

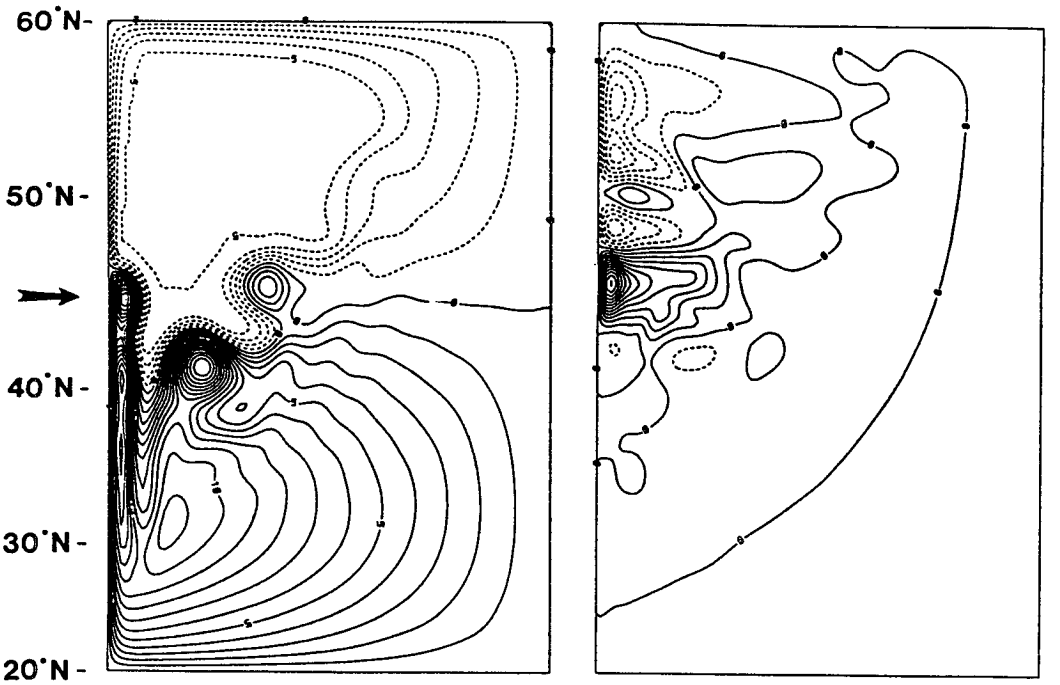

FIG. 4. Five-year time-average mass transport streamfunctions for E1. (a) Upper-layer, contour interval of 1 Sv; (b) lower layer, contour interval of 0.5 Sv.

which is now more than doubled to 0.34 by a decrease in the initial upper-layer thickness to 100 m (Table 1).

As expected, the outcrop region increases in size and, because of the larger λ, the upper-layer circulation is more intense. The resulting 5-year time-average streamfunctions are displayed in Fig. 5. As in E1, the flow patterns are characteristic of the instantaneous ones and can therefore be considered a standing pattern. The oscillating wave or loop current of E1 is still present, but the separation latitude is now farther north of the ZWCL. The recirculation within the loop is small and, as in E1, a recirculation is also present within the second oscillation in the midlatitude jet. As will be shown in section 4, the vorticity changes in both E1 and E2 are occuring first within the loop current and then within this secondary recirculation. The lower-layer circulation (Fig. 5b) is now more intense than that of E1, as the outcrop area (i.e., the region of direct forcing) is larger.

In summary, a shift toward a flow pattern exhibiting a recirculation gyre did not occur in these experiments with a doubling of λ. On the contrary, in that case the loop current extends farther to the north.

b. *The "inertial recirculation" regime—λ = 1.35*

In E3, λ is increased to 1.35 by reducing the initial upper-layer thickness to 50 m, an almost tenfold increase from its value in E1. As for E1 and E2, E3 was integrated for a 5-yr period after a 10-yr spinup. The flow pattern differs drastically from E2 as the loop current is no longer present and a strong recirculation [maximum transport of 31 Sv ($Sv \equiv 10^6\ m^3\ s^{-1}$)] now appears next to the western boundary. The 5-year time-average upper-layer streamfunction is shown in Fig. 6a. The midlatitude jet now separates far south of the ZWCL at approximately 25°N. No oscillating wave is present. The circulation (Fig. 6b) in the lower layer is the classic two-gyre pattern as most of the layer is now directly wind forced. In summary, with an almost tenfold increase in λ from E1, we are able to observe a shift from a regime with a loop current regime to one with a strong inertial recirculating gyre.

c. *Importance of λ*

In the experiments discussed above, the parameter λ was gradually increased by decreasing the initial upper-layer thickness. While the vertically integrated Sverdrup transport remained constant from one experiment to the other, the Rossby radius of deformation [$\sim (g'H_1)^{1/2}/f$] decreased.

To illustrate the fact that λ is effectively a characteristic of the above circulation patterns despite the nonlinearity of the solution, two more experiments, E4 and E5 (not illustrated), were performed in which the increase in λ was achieved by respectively doubling and quadrupling the magnitude of the wind stress τ_m, therefore leading to λ values of 0.3 and 0.6. The Rossby radius of deformation then remains constant from one

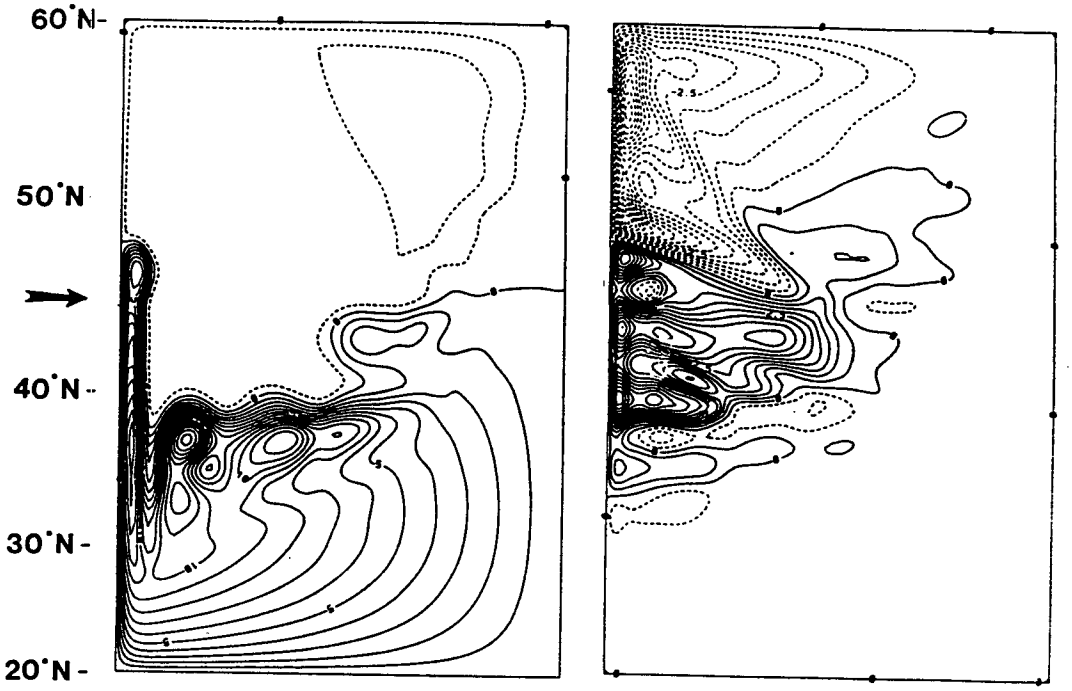

FIG. 5. Five-year time-average mass transport streamfunctions for E2. (a) Upper layer, contour interval of 1 Sv; (b) lower layer, contour interval of 0.5 Sv.

experiment to the other, but not the corresponding vertically integrated Sverdrup transport, as in the case of E1, E2, and E3. However, the flow patterns do evolve as from E1 to E3 as λ is increased: for a doubling in magnitude of the wind stress in E4 ($\lambda = 0.3$), the upper-layer flow pattern is almost identical to E2; a further doubling in E5 ($\lambda = 0.6$) leads to a recirculation regime, similar to E3, but with a smaller outcrop area and an oscillating wave. In summary, in the context of this two-layer nonlinear model, λ effectively characterizes the flow pattern as surmised by Veronis (1973) and Huang (1984).

4. Impact of layer outcropping on vorticity dissipation

To discuss and interpret the above flow patterns, it is useful to introduce some characteristic scales. In the linear limit, for weak forcing or large viscosity, the boundary layer thickness is given by the Munk scale

$$\delta_M = \left(\frac{A}{\beta}\right)^{1/3}. \tag{3}$$

In the nonlinear limit, for strong forcing or small viscosity, the boundary layer thickness is given by the inertial scale

$$\delta_I = \left(\frac{U}{\beta}\right)^{1/2}, \tag{4}$$

where U is the magnitude of the interior zonal flow.

For a 1½-layer model, $U = g'H_1/fL$, and, when applied to the parameters of experiment E1 (Table 1), the above scales are $\delta_M \approx 30$ km and $\delta_I \approx 40$ km, giving a ratio $\delta_I/\delta_M \approx 1.3$. Experiment E1 is therefore less inertial that CCY and Cessi's (1991) "pivot" case ($\delta_I/\delta_M \approx 4$). However, before any occurence of layer outcropping (Figs. 3a,b), the upper-layer circulation of E1 exhibits standing Rossby waves having similar characteristics as the ones obtained by CCY and Cessi (1991) in their investigation of the steady barotropic circulation driven by inflow–outflow boundary conditions in a rectangular β-plane domain. Despite the fact that our solution is baroclinic, a good qualitative agreement is obtained in the absence of outcropping layers after one and three year integrations, respectively. In the first case, both northward flowing western boundary currents reach the northern wall where a small recirculation gyre forms (run 4 of CCY). In the second case, the weak southward western boundary current in E1 is sufficient to drive a small recirculation within the loop current as illustrated by Fig. 9 of Cessi (1991). Quantitative differences are observed such as a shorter eastward penetration and a faster decay. This is in agreement with the fact that E1 is less inertial than CCY's cases as illustrated by the following scale analysis.

While objections have been raised against Moore's (1963) scenario (Il'in and Kamenkovich 1964; Ierley and Ruehr 1986; Ierley 1987), his basic scale analysis

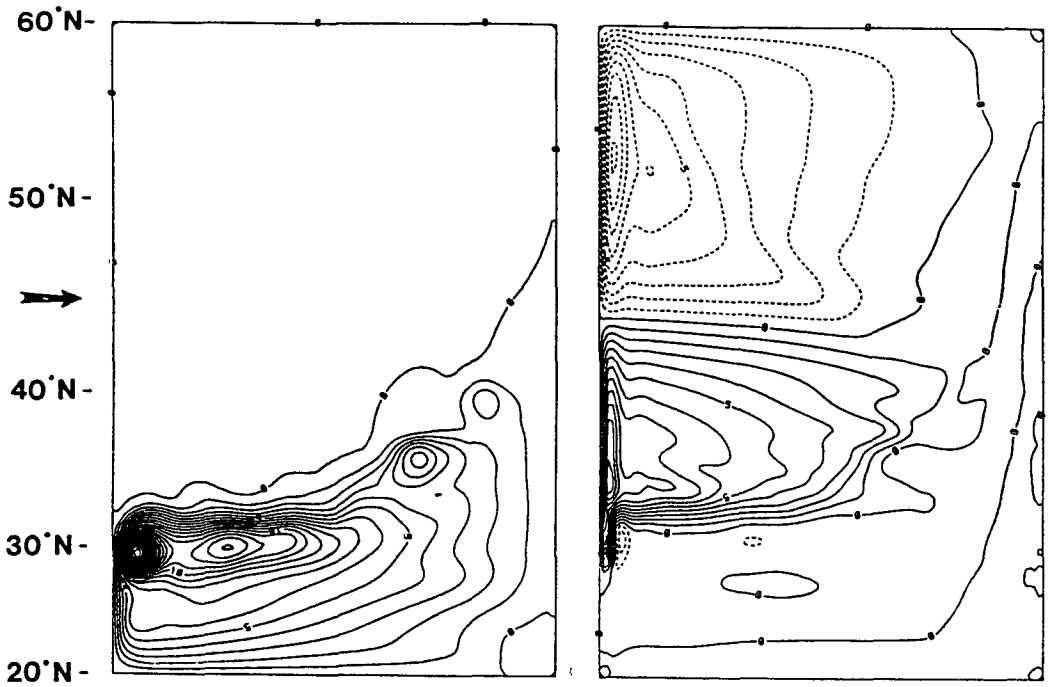

FIG. 6. Five-year time-average mass transport streamfunctions for E3. (a) Upper layer; (b) lower layer. The contour interval is 1 Sv.

remains valid and has been used extensively by CCY to discuss and interpret their results. The standing Rossby wave needed to close the potential vorticity balance then possesses a wavelength L equal to $2\pi\delta_I$ and is slowly damped by friction with a number of oscillations of the order of $(\delta_I/\delta_M)^3$ (Pedlosky 1987). When applied to the parameters of E1, $L \approx 300$ km and the number of oscillations before decay is given by $N \approx 2$. In E1, the actual wavelengths of the oscillating Rossby waves in both Figs. 3a,b are of the order of 350 km and decay after two oscillations, agreeing with the above scaling and the findings of CCY.

As soon as the upper-layer outcrops in E1, only the first oscillation (the loop current) remains. While the wavelength corresponding to this oscillation is still in agreement with the above scaling, the combination of layer outcropping and transients alters the standing Rossby wave pattern (Fig. 4a). As already stated, vorticity dissipation in the western boundary current region is insufficient to balance the vorticity input by the wind stress. The vorticity transformations for E1 are illustrated in Fig. 7a, which displays the vertically integrated relative vorticity over the domain in analogy with the barotropic experiments of CCY. In agreement with CCY, most of the largest transformations in vorticity occur within the loop current, but they also occur within the secondary recirculation.

In E2, for a doubling of λ from E1, the oscillating wave extends farther north despite the larger outcrop area. As in E1, a recirculation is also present within the second oscillation (Fig. 5a), and the vorticity changes, as illustrated in Fig. 7b, occur also in the loop current and within the recirculation. That the northward overshoot lengthens in E2 is consistent with the findings of CCY, who state that most of the dissipation occurs there and not in the wave as the fluid approaches the interior of the domain. Killworth (1993), on the other hand, found that the dissipation instead occurs in the wave as stated by Pedlosky (1987). In Killworth (1993), the dissipation is achieved with a linear drag instead of the higher-order friction law used by CCY and this study. This is of importance on the dissipation process as illustrated by Böning (1986). The vorticity equation integrated over a domain D enclosed by a streamline and over the total fluid depth H is given by

$$\frac{1}{H}\int\int_D \mathrm{curl}\tau dxdy = -A\int\int_D \nabla^2\zeta dxdy + \sigma\int\int_D \zeta dxdy. \quad (5)$$

If the circulation is in equilibrium, the vorticity input from the wind into any domain D must be balanced by the model dissipation process. If the vorticity loss is expressed by a high-order friction law as in the numerical model and in CCY, a strong recirculation with large vorticity ζ can occur as long as the distribution of $\nabla^2\zeta$ balances the wind input. This is not possible if the friction law is expressed only as a linear drag.

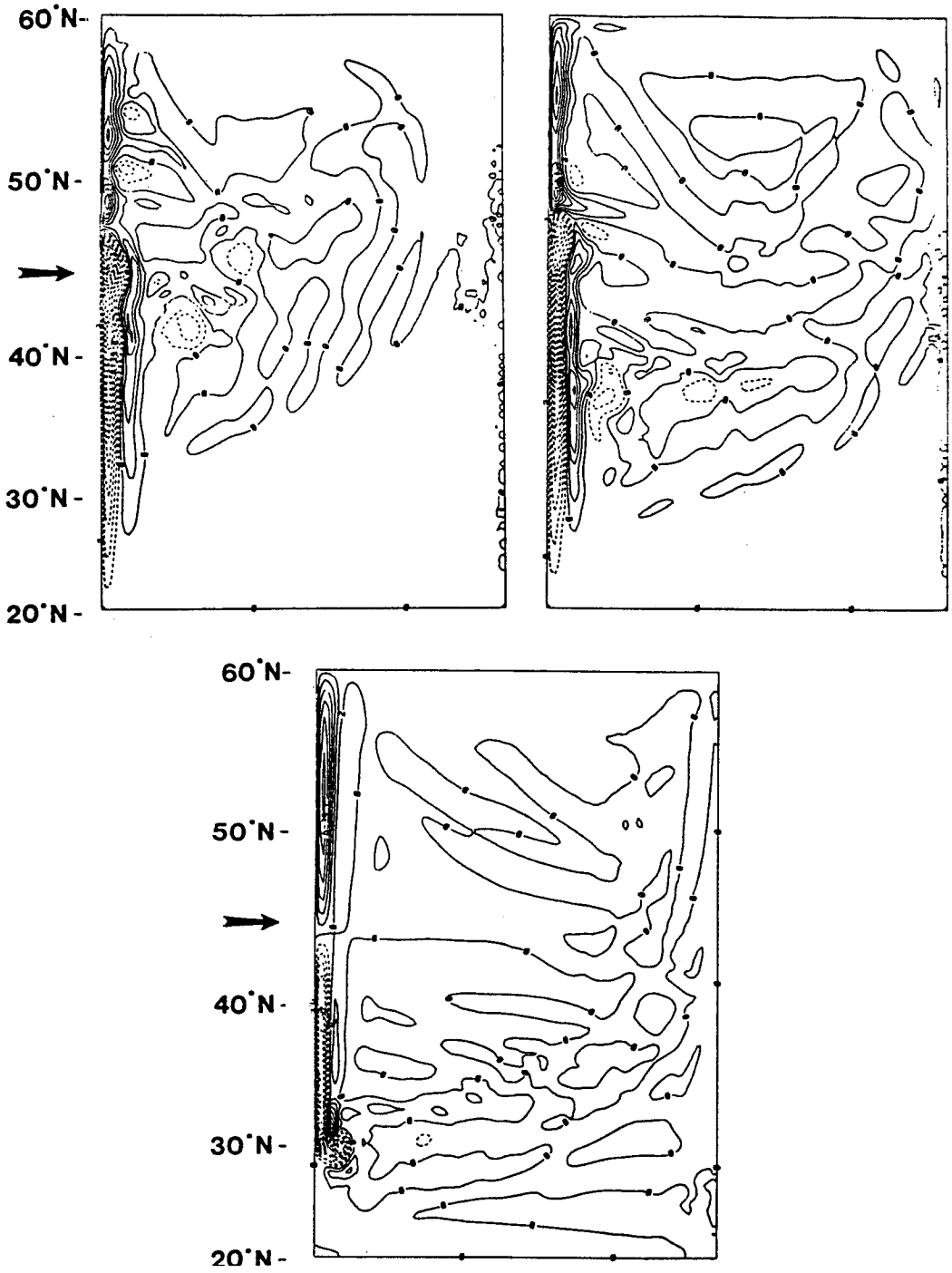

FIG. 7. Vertically integrated vorticity fields for (a) E1, (b) E2, and (c) E3. The contour interval is 2.5×10^{-6} s^{-1}.

In E3, the upper-layer flow becomes more inertial as both λ and δ_I increase (Table 1). The upper-layer flow pattern then varies drastically as described in the previous section. The loop current regime is completely replaced by a tight recirculation (Fig. 6a) where most of the vorticity changes take place (Fig. 7c). Dissipation (not illustrated), that is, diffusion of vorticity out of the area bounded by a streamline, occurs as in Böning (1986) along the boundary and midlatitude jets. Outside the recirculation area, negative vorticity is actually diffused inward and accelerates the recirculating gyre. For more detail on the processes at work, the reader is referred to Böning (1986).

In summary, as surmised in section 3, most of the vorticity transformations take place within 1) the first oscillating wave in the case of a loop current regime and 2) the recirculating gyre in the case of a recirculation regime.

5. Influence of baroclinic instabilities

In analogy to the barotropic experiments of CCY and Cessi (1991), only the vertically integrated vorticity patterns were discussed in section 4, as a function of the upper-layer flow patterns. The upper to lower layer ratio ($\delta = H_1/H_2$) of these experiments is very small (less than 10^{-4}). According to the criterion derived by Chassignet and Cushman-Roisin (1991), this small ratio is equivalent to a dynamically inactive second layer and to no baroclinic instabilities. This criterion naturally applies only when the upper-layer thickness is nonzero and, consequently, when the lower layer is not directly forced by the wind.

In the case of motion confined to the upper layer, that is, a quiescent bottom layer, Fofonoff (1962) and Cessi (1990) predict a large recirculating gyre that is completely specified by the initial choice of potential vorticity, assumed to be constant in the recirculation region (Cessi et al. 1987). This is, however, not in agreement with experiment E3 and E5 of section 3, both of which exhibit a tight recirculation close to the western boundary. One may attribute the differences in behavior to the fact that no area of uniform potential vorticity is present in either E3 or E5 (Fig. 8).

With an "infinitely" deep lower layer, baroclinic instabilities are precluded. They will, however, occur if the lower layer is shallow enough to be set in motion so as to reduce the vertical shear associated with the separated current (Rhines and Young 1982; Cessi 1990; Chassignet and Cushman-Roisin 1991). Furthermore, Cessi (1990) postulated the presence of a depth-independent barotropic core in the recirculating gyre. To investigate the importance of baroclinic instabilities on the vertical structure of the recirculation, a series of experiments identical to those of section 3, with the exception of a total basin depth of 5000 m, was performed (Table 1). The upper to lower layer ratio δ therefore varies from $1/30$ for E1s, E4s, and E5s to $1/50$ for E2s and $1/100$ for E3s. For all experiments, the upper-layer flow patterns (not illustrated, except for E5s) retained the same characteristics of the "infinitely" deep lower-layer experiments, except that in E1s, E2s, and E4s the secondary recirculation located east of the loop current disappeared. Of particular interest is experiment E5s, which does exhibit a barotropic component in the recirculating gyre (Fig. 9). The velocities are not, however, depth independent as one would expect from Cessi's (1990) analytical solution. The lower-layer recirculation is less intense, as it possesses the same transport as the upper one over a much thicker layer. In E3s, despite a larger λ, the lower layer remains

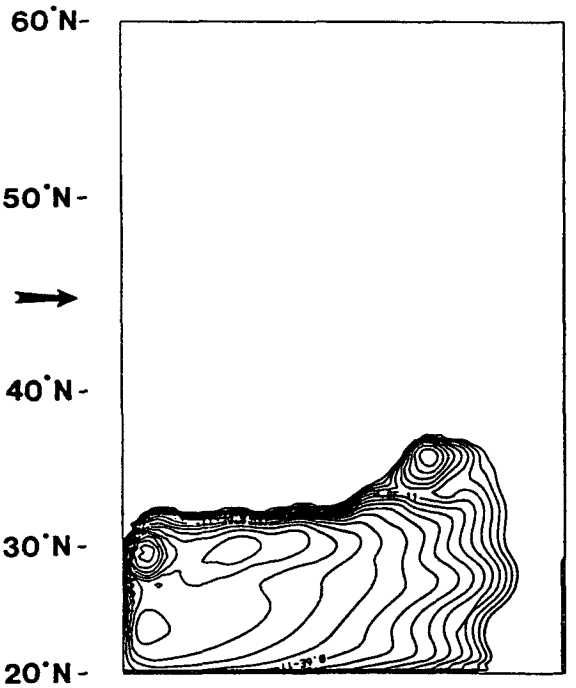

FIG. 8. Upper-layer potential vorticity fields for E3. The contour interval is 10^{-10} m^{-1} s^{-1} and the contours higher than 10^{-6} m^{-1} s^{-1} are not shown.

quiescent as the small δ still precludes baroclinic instabilities. In E1s, E2s, and E4s a small recirculating gyre is also found in the lower layer beneath the upper recirculation located in the loop current.

In experiments that allow for both a recirculating gyre and baroclinic instabilities, such as E5s, the numerical solutions differ significantly from the analytical work of Cessi (1990) in the sense that the flow within the recirculating gyre is not entirely depth independent. Several factors can readily be advanced to explain these discrepancies. Potential vorticity is assumed by Cessi (1990) to be rendered uniformed in the boundary current region by the eddy field. Wind forcing is assumed to be negligible with respect to eddy processes. However, Chassignet and Bleck (1993) showed that homogenized potential vorticity is primarily confined to regions isolated from forcing and dissipation. This homogenization occurs only in interior layers, as illustrated by the six-layer experiment of Chassignet and Bleck (1993). In that experiment, the recirculation, although not barotropic, is found to extend all the way to the bottom, as illustrated by the meridional velocity cross section of Fig. 10.

6. Influence of boundary conditions

In this section, we address the impact upon the different regimes of the choices made in boundary conditions. In particular, we are interested in 1) the lateral

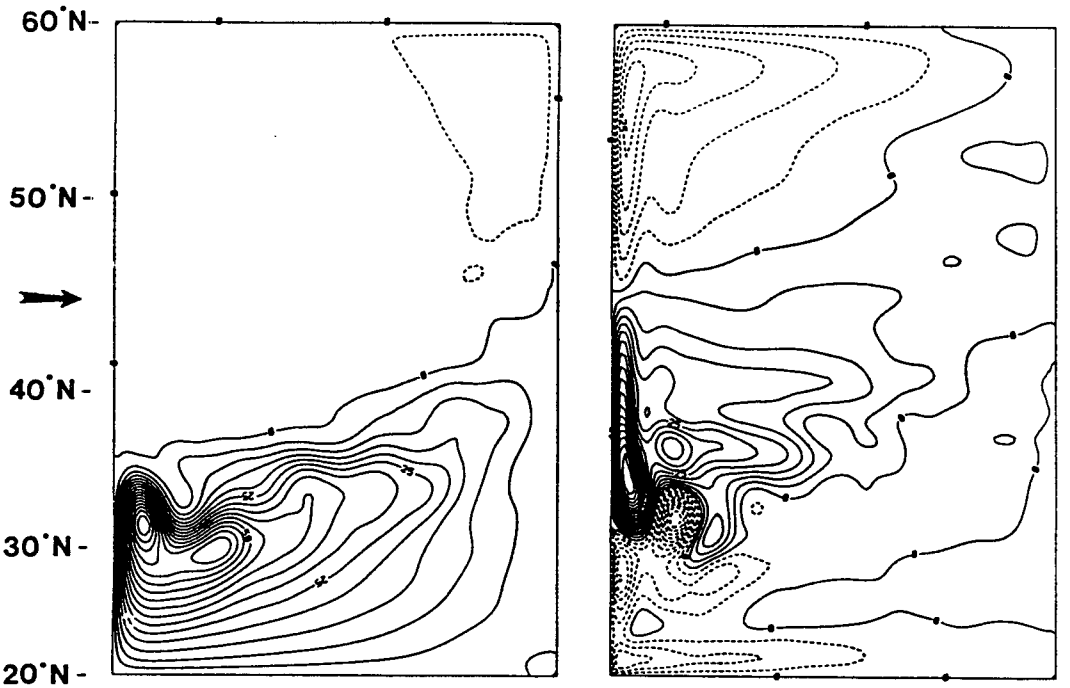

FIG. 9. Five-year time-average mass transport streamfunctions for E5s. (a) Upper layer; (b) lower layer. The contour interval is 5 Sv.

boundary condition, that is, free slip versus no slip, which is known to be of importance in the separation of western boundary currents (Haidvogel et al. 1992), and 2) bottom friction, which has been shown to be of importance in the dissipation process (Böning 1986).

a. Lateral boundary conditions

Haidvogel et al. (1992) illustrated the transition that occurs in flow patterns as the boundary conditions are continuously varied from free slip to no slip. The no-slip case was characterized by an early separation south of the ZWCL. Furthermore, Cessi (1991) was able to obtain a recirculating gyre regime *only* when no-slip boundary conditions were specified on the western boundary. When free slip was prescribed, for experiments having the same parameters, the western boundary currents separated close to the northern boundary with no recirculating gyre. On the other hand, in this study, all experiments discussed to this point have been performed with free-slip boundary conditions *only*. Nonetheless, a recirculation regime was obtained for high λs. In the two-layer system, the separation is associated with the outcropping of the upper layer, which is a large-scale response dependent on integral properties of the applied wind stress (Parsons 1969; Veronis 1973; Huang 1984; Chassignet and Bleck 1993). Presumably, the separation is then independent of the choice made for the lateral boundary conditions. This may not be the case for a large overshoot.

To investigate the impact of the lateral boundary conditions on the two regimes, experiments E2s and E5s were integrated with no-slip boundary conditions becoming experiments E2n and E5n, respectively. There is no overshoot present in the upper-layer circulation of E5s (Fig. 9a), and the differences with E5n (not illustrated) are negligible. The western boundary currents separate at the same location in both experiments. The choice of the lateral boundary condition is therefore not crucial. This result then supports the idea that the outcropping mechanism is the major factor affecting the separation. On the other hand, E2n (Fig. 11) differs drastically from E2 (Fig. 5). Here the change in boundary conditions did provide a shift from a loop current regime to a recirculation one. This is in agreement with Cessi's (1991) results, which state that when a no-slip boundary condition is used, vorticity is generated in the viscous sublayer and deceleration triggers the separation. These results are also in agreement with Killworth (1993), who states that "the western boundary layer structures do not require that the ocean interior be related to the dynamics of the boundary layer itself." In the two-layer model, the degree to which they are dependent is a function of the nonlinearity of the solution.

In summary, in a two-layer system, separation is independent of the choice of lateral boundary conditions as long as λ is large enough to generate a dissipation regime with a recirculation for either boundary condition, that is, free slip or no slip. If λ is not suffi-

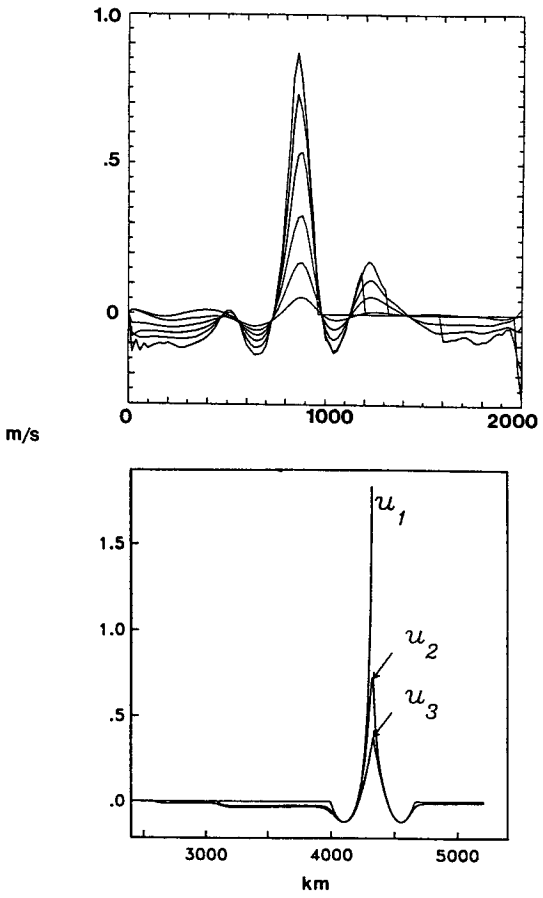

FIG. 10. (a) Meridional velocity profile across the recirculating gyre for the six-layer experiment of Chassignet and Bleck (1993) (symmetric wind forcing, square domain 2000 km × 2000 km) and (b) analytical velocity profile for a three-layer system from Cessi (1990).

ciently large, despite the fact that the total outcrop area is a function of the integral properties of the applied wind stress, an overshoot will be present when a free-slip boundary condition is prescribed.

b. Bottom drag

In the barotropic context of a single gyre domain, Böning (1986) showed that, as long as lateral diffusion dominates bottom friction, a strong recirculating gyre regime will be present. If bottom friction is dominant (Veronis 1966), an inertial recirculation will exist only for large Rossby numbers. It is therefore of interest to explore the impact of small bottom friction (2.65×10^{-7} s^{-1}) applied as a linear law in the bottom layer [Eq. (1) of section 2]. When applied to the experiments of section 5 (total depth of 5000 m), the impact on the upper-layer circulation is minor. In the lower layer, however, the intensity of the circulation is reduced. In the case of a recirculating gyre regime, this increases the differences in velocity between the upper and lower recirculation, consequently carrying the numerical solution even farther away from the depth-independent state of Cessi (1990). The barotropic component remains present, however.

7. Influence of coastline orientation

All the experiments reported in the previous section were configured in a rectangular domain with a north–south western boundary. In cases with a tight recirculation near the western boundary such as E3 or E5, the question arises as to whether coastline orientation can actually modify this pattern. This is of particular interest as a tight recirculation similar to the one in E3 and E5 can be seen in full GCMs as illustrated by Fig. 1. The numerical model of section 2 was therefore reconfigured with a realistic coastline of the North Atlantic. The domain area not covered by land is approximately the same as in the rectangular experiments. This corresponds to a North Atlantic Ocean approximately 30% smaller than in reality. A one-year time average of the upper-layer thickness after 12 years of integration is displayed in Fig. 12 for forcing identical to E5. In addition to a western boundary current separation located at approximately Cape Hatteras, the flow pattern exhibits a recirculation now elongated along the Gulf Stream and no longer close to the western boundary. This experiment is only meant to illustrate the possible importance of coastline orientation. For a more detailed discussion on the impact of coastline orientation on separation and current extension, the reader is referred to recent work by Campos and Olson (1991), who included time dependency to the analytic treatment of Moore (1963) and Pedlosky (1987); by Dengg (1993), who performed a barotropic study of the Gulf Stream separation; and by Agra and Nof (1993), who analyzed the collision and separation of western boundary currents in a $2\frac{1}{2}$-layer analytical model.

8. Summary and discussion

In an exploration of the dynamics of current separation and vorticity dissipation in a two-layer model, it was found that 1) results obtained in a barotropic context remain valid, namely, that two major dissipation regimes can be found, either a loop current or a recirculating gyre; 2) a transition from one regime to the other can be achieved if one increases the strength of the front associated with the outcrop, regardless of the specified boundary conditions; and 3) separation will depend upon the choice of lateral boundary conditions if the upper-layer flow is not highly inertial.

The experiments described in this paper were aimed at developing an understanding of the jet separation and associated recirculation in large-scale eddy-resolving simulations, since most realistic experiments to date

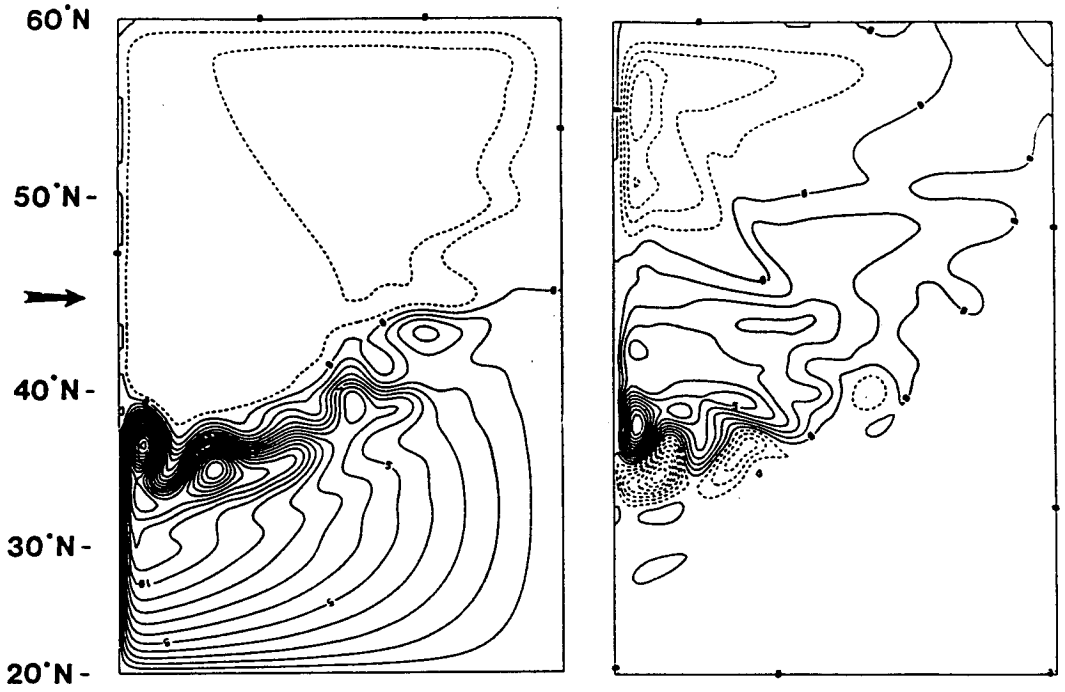

FIG. 11. Five-year time-average mass transport streamfunctions for E2n. (a) Upper layer; (b) lower layer. The contour interval is 1 Sv.

not only have a midlatitude jet that overshoots the ZWCL but also develop an intense recirculation eddy near the coast (Thompson and Schmitz 1989; Beckmann et al. 1994). In a series of barotropic experiments, Cessi (1991) discussed the different possible dissipation regimes as a function of the relative strength of two colliding jets. A weak southward flowing jet favored a loop current dissipation, while a strong jet induced a strong recirculating gyre.

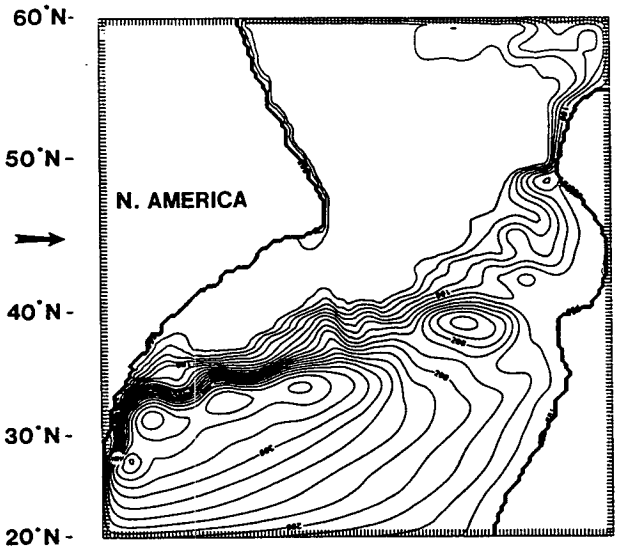

FIG. 12. One-year time average of the upper-layer thickness for an experiment with a realistic coastline. The parameters are the same as for experiment E5s. The contour interval is 20 m.

Inclusion of baroclinicity as reported in this paper does alter the separation mechanism found in the barotropic experiments. However, the results must be viewed in the context of a two-layer model. A similar series of experiments performed with a multilevel numerical model may behave differently, as discussed by Chassignet and Gent (1991). The location of the midlatitude jet separation is dependent upon the choice made in the model formulation, that is, layers versus levels, and that the wind forcing is prescribed as a body force acting only on the upper layer/level. The formulation of the lateral boundary conditions was also found to be of importance. In the experiments reported in this paper, the circulation is also highly sensitive to the stratification choices since the wind forcing acts only on the layer in direct contact with the atmosphere.

In the ocean, the depth over which the wind acts is time and space dependent and is usually assumed to be the depth of the mixed layer. Without thermodynamics in the model, the amount of fluid in the upper layer is fixed. This amount, together with the wind-forcing formulation, dictates the outcrop location and size as well as the form of the dissipation regime. This naturally raises the question regarding the extent to which the midlatitude jet separation mechanism with outcropping layers is modified by the presence of a thermodynamically active mixed layer. The addition

of a mixed layer (Bleck et al. 1989) will remove the ambiguities associated with distributing the wind forcing over various layers. Other diabatic effects such as deep water formation and diapycnal mixing are also likely to have an impact on the midlatitude jet separation. Finally, we must consider the impact of bottom topography. Both the impact of a mixed layer and of topography are presently under investigation.

Acknowledgments. Discussions with C. Böning, P. Cessi, W. Holland, C. Rooth, and G. Veronis proved timely and valuable. Support was provided by the Office of Naval Research under Contract NOOO14-93-1-0404. Computations were carried out using the CRAY Y-MP at the National Center for Atmospheric Research (NCAR). NCAR is sponsored by the National Science Foundation.

REFERENCES

Agra, C., and D. Nof, 1993: Collsion and separation of boundary currents. *Deep-Sea Res.*, **40,** 2259–2282.

Beckmann, A., C. W. Böning, C. Köberle, and J. Willebrand, 1994: Effects of increased horizontal resolution in a simulation of the North Atlantic Ocean. *J. Phys. Oceanogr.*, **24,** 326–344.

Bleck, R., and D. B. Boudra, 1986: Wind-driven spin up in eddy-resolving ocean models formulated in isopycnic and isobaric coordinates. *J. Geophys. Res.*, **91,** 7611–7621.

——, H. P. Hanson, D. Hu, and E. B. Kraus, 1989: Mixed layer/thermocline interaction in a three-dimensional isopycnal model. *J. Phys. Oceanogr.*, **19,** 1417–1439.

Böning, C. W., 1986: On the influence of frictional parameterization in wind-driven ocean circulation models. *Dyn. Atmos. Oceans,* **10,** 63–92.

Boris, J. P., and D. L. Book, 1973: Flux-corrected transport. I. SHASTA, a fluid transport algorithm that works. *J. Comput. Phys.*, **11,** 38–69.

Bryan, K., 1963: A numerical investigation of a nonlinear model of a wind-driven ocean. *J. Atmos. Sci.*, **20,** 594–606.

Campos, E. J. D., and D. B. Olson, 1991: Stationary Rossby waves in western boundary current extensions. *J. Phys. Oceanogr.*, **21,** 1202–1224.

Cessi, P., 1990: Recirculation and separation of boundary currents. *J. Mar. Res.*, **48,** 1–35.

——, 1991: Laminar separation of colliding western boundary currents. *J. Mar. Res.*, **49,** 697–717.

——, G. R. Ierley, and W. R. Young, 1987: A model of inertial recirculation driven by potential vorticity anomalies. *J. Phys. Oceanogr.*, **17,** 1640–1652.

——, R. V. Condie, and W. R. Young, 1990: Dissipative dynamics of western boundary currents. *J. Mar. Res.*, **48,** 677–700.

Chassignet, E. P., and B. Cushman-Roisin, 1991: On the influence of a lower layer on the propagation of nonlinear oceanic eddies. *J. Phys. Oceanogr.*, **21,** 939–957.

——, and P. R. Gent, 1991: The influence of boundary conditions on midlatitude jet separation in ocean numerical models. *J. Phys. Oceanogr.*, **21,** 1290–1299.

——, and R. Bleck, 1993: The influence of layer outcropping on the separation of boundary currents. Part I: The wind-driven experiments. *J. Phys. Oceanogr.*, **23,** 1485–1507.

Dengg, J., 1993: The problem of Gulf Stream separation: A barotropic approach. *J. Phys. Oceanogr.*, **23,** 2182–2199.

Fofonoff, N. P., 1962: Dynamics of ocean currents. *The Sea: Ideas and Observations in the Study of the Seas,* Vol. 1, M. N. Hill, Ed., Wiley-Interscience, 323–395.

Haidvogel, D. B., J. L. Wilkin, and R. Young, 1991: A semi-spectral primitive equation ocean circulation model using vertical sigma and orthogonal curvilinear horizontal coordinates. *J. Comput. Phys.*, **94,** 151–185.

——, J. C. McWilliams, and P. R. Gent, 1992: Boundary current separation in a quasigeostrophic, eddy-resolving ocean circulation model. *J. Phys. Oceanogr.*, **22,** 882–902.

Hogg, N. G., 1992: On the transport of the Gulf Stream between Cape Hatteras and the Grand Banks. *Deep-Sea Res.*, **39,** 1231–1246.

Holland, W. R., and L. B. Lin, 1975: On the generation of mesoscale eddies and their contribution to the oceanic general circulation. Parts I and II. *J. Phys. Oceanogr.*, **5,** 642–669.

Huang, R. X., 1984: The thermocline and current structure in subtropical/subpolar basins. Ph.D. thesis, WHOI-84-42, 218 pp.

——, and G. Flierl, 1987: Two-layer models for the thermocline and current structure in subtropical/subpolar gyres. *J. Phys. Oceanogr.*, **17,** 872–884.

Ierley, G. R., 1987: On the onset of inertial recirculation in barotropic general circulation models. *J. Phys. Oceanogr.*, **17,** 2366–2374.

——, and O. G. Ruehr, 1986: Analytic and numerical solutions of a nonlinear boundary layer problem. *Stud. Appl. Math.*, **75,** 1–36.

Il'in, A. M., and V. M. Kamenkovich, 1964: The structure of the boundary layer in the two dimensional theory of ocean currents. *Okeanologiya,* **5,** 756–769.

Killworth, P. D., 1993: On the role of dissipation in inertial western boundary currents. *J. Phys. Oceanogr.*, **23,** 539–553.

McWilliams, J. C., N. J. Norton, P. R. Gent, and D. B. Haidvogel, 1990: A linear balance model of wind-driven, midlatitude ocean circulation. *J. Phys. Oceanogr.*, **20,** 1349–1378.

Moore, D. W., 1963: Rossby waves in ocean circulation. *Deep-Sea Res.*, **10,** 735–747.

Parsons, A. T., 1969: A two-layer model of Gulf Stream separation. *J. Fluid Mech.*, **39,** 511–528.

Pedlosky, J., 1987: *Geophysical Fluid Dynamics.* 2d ed. Springer-Verlag, 624 pp.

Rhines, P. B., and W. R. Young, 1982: Homogenization of potential vorticity in planetary gyres. *J. Fluid Mech.*, **122,** 347–367.

Sun, S., R. Bleck, and E. P. Chassignet, 1993: Layer outcropping in numerical models of startified flows. *J. Phys. Oceanogr.*, **23,** 1877–1884.

Thompson, J. D., and W. J. Schmitz, 1989: A limited-area model of the Gulf Stream: Design, initial experiments, and model-data intercomparison. *J. Phys. Oceanogr.*, **19,** 791–814.

Veronis, G., 1966: Wind-driven ocean circulation—Parts 1 and 2. *Deep-Sea Res.*, **13,** 17–55.

——, 1973: Model of World Ocean circulation: I. Wind-driven, two-layer. *J. Mar. Res.*, **31,** 228–288.

Zalesak, S. T., 1979: Fully multidimensional flux-corrected transport algorithms for fluids. *J. Comput. Phys.*, **31,** 335–362.